

Contents lists available at ScienceDirect

Composite Structures

journal homepage: www.elsevier.com/locate/compstruct



Applicability of two-step homogenization to high-crimp woven composites



Higor Galdino da Silva^a, Kostiantyn Vasylevskyi^b, Borys Drach^{a,*}, Igor Tsukrov^b

- ^a Mechanical & Aerospace Engineering, New Mexico State University, Las Cruces, NM, United States
- ^b Mechanical Engineering, University of New Hampshire, Durham, NH, United States

ARTICLE INFO

Keywords:
Homogenization
Woven composites
Finite element analysis
Microtomography processing
Crimp ratio
Periodic boundary conditions

ABSTRACT

This paper examines applicability of a two-step homogenization approach to carbon/epoxy 3D woven composites. The first step of this approach involves microscale homogenization of the reinforcement consisting of wavy bundles of fibers. Finite Element Analysis (FEA) is used to obtain homogenized properties of explicitly modeled and homogenized wavy tows with fiber volume fraction of 70%. Two geometric parameters are investigated: crimp ratio and wavelength normalized by fiber diameter. Effective elastic properties are shown to be sensitive to the normalized wavelength parameter up to the value 50 at which point they reach asymptotic values and the separation of scales can be claimed.

The resulting homogenized properties of the wavy tows are used to calculate the effective elastic properties of one high-crimp and two low-crimp 3D woven composites using FEA. The results of the numerical two-step homogenization are compared with experimental data and a simple Voigt model. Good correlation is observed between experimental results and the homogenization based on direct FEA. The considered Voigt approximation may be used as a reasonable first order estimate for Young's moduli in low-crimp woven composites.

1. Introduction

The ever-increasing demand for lighter and stronger materials has pushed the development of woven composites that are now used extensively in aerospace industry. Manufacturers of such composite materials have been using finite element analysis (FEA) to study the materials' responses under various loading and environmental conditions with the purpose of getting the best performance out of the products. However, 3D woven composites, in particular, are difficult to model and analyze due to the complicated shape of the reinforcement fiber tows (bundles of fibers). Moreover, each tow contains thousands of transversely isotropic fibers, which makes it almost impossible to represent the tows explicitly in numerical modeling. The standard way of dealing with this complication is to apply homogenization theories, e.g. Hashin, Chamis, Hashin-Shtrikman bounds, etc., in order to obtain effective mechanical properties of tows and model them as solid homogeneous objects [1-5]. As a result, the composite material is often represented by two solid phases - matrix and homogenized tows - and a unit of the entire composite (unit cell) can then be analyzed to determine the overall properties. Such a two-step approach has been demonstrated to work for laminates with unidirectional layers [6,7], twodimensional (2D) woven composites [8], and three-dimensional (3D)

woven composites with limited through-thickness reinforcement [9,10]. However, a study focusing on the applicability of the approach to highly crimped 3D woven composites has not been performed to the best of the authors' knowledge.

The authors in [11-13] study the elastic response of periodic wavy tow unit cells having sinusoidal shapes with explicitly modeled transversely isotropic fibers under small strain using FEA. In [11] they focus on the effective elastic properties of wavy tows with different crimp ratios (0-0.10) and different fiber volume fraction values (0.40-0.70). They conclude that increasing the tow waviness drastically reduces the Young's modulus in the longitudinal direction - average reduction of 70% at crimp value of 0.10 compared to straight fibers. In addition, they show that at different fiber volume fractions the reduction of the effective Young's moduli follows the same pattern. In [13], the effect of waviness on the effective coefficients of thermal expansion (CTE) of tows is investigated. The authors observe an increase in the longitudinal CTE and little to no decrease in the transverse CTE. Furthermore, in [14] the effects of crimp ratio, fiber arrangement and fiber wavelength normalized by the fiber diameter are discussed in the context of large deformation of composites with wavy fiber. However, none of these studies address effect of the normalized wavelength on elastic proper-

E-mail address: borys@nmsu.edu (B. Drach).

^{*} Corresponding author at: Mechanical and Aerospace Engineering, New Mexico State University, P.O. Box 30001, MSC 3450, Las Cruces, NM 88003-8001, United States.

H. Galdino da Silva, et al. Composite Structures 226 (2019) 111157

Other groups have focused on estimating effective properties of woven composites based on tow geometry and the homogenized properties of tows found using common homogenization techniques [15-18]. However, such homogenization techniques do not account for the effect of the fiber diameter-to-length ratio on the homogenized properties: the tows are assumed to be infinitely long, i.e. fiber length is much greater than diameter. The authors in [19] approximate a plain weave architecture as an assemblage of tows modeled as homogenized solid objects with paths having zig-zag, trapezoidal, and helical shapes. The trapezoidal model is the one that provides good estimation of Young's Moduli (E) compared to experimental data – 7.1% maximum error in the through-thickness direction. Authors in [20] propose an analytical model for the plain weave architecture and model the tows as homogenized solids with elliptical cross-section shape and tow paths represented either by a series of circular arcs or sinusoids. An analytical approximation method is proposed by [21] to describe the elastic properties of an orthogonal woven composite. In this method the composite unit cell is subdivided into layers and for each layer the elastic properties are estimated based on a weighted average of the stiffness components of each tow (warp, weft, and binder) and matrix. The approximation results in overestimated predictions for all values of the Young's moduli - 12.87% in the warp direction, 4.91% in the transverse in-plane direction, and 36.82% in the through-thickness direction.

Several groups have performed elastic homogenization of 2D and 3D woven composites using FEA. It has been shown by [22-25] that homogenization of woven composites improves with more accurate tow geometry characterization. The authors in [22] estimate the longitudinal Young's moduli of a 3D woven textile composite with 11-13% accuracy compared to the experimental data. Using similar geometries, [23] refine the mesh and locally correct homogenized material properties of the tows. As a result, the authors obtain even closer values for longitudinal Young's moduli: 0.1% best case and 13% worst case when compared with the experimental data. Another realistic modeling done by [25] shows better correspondence between the microtomographyinformed model and experimental data (relative error $\delta E_1 = -11\%$, and $\delta E_2 = 0.2\%$) than the idealized geometry which produced overestimated predictions (relative error $\delta E_1 = 14\%$, and $\delta E_2 = 17\%$). FEA homogenization of a 2D woven composite in [9] yields good approximation of the effective in-plane moduli compared to the averaged experimental results (relative error of 3.1% in both warp and weft directions). A plyto-ply architecture is modeled in [26] and the FEA results are within 12% of the averaged experimental results in the weft direction. In [10] the authors investigate homogenized mechanical properties of an orthogonal architecture based on two FEA methods: conventional (no mesh overlapping), and mesh superposition method. Both FEA methods result in close approximation of the experimental results: conventional - in-plane moduli are within 6.2-8.0% relative error range; mesh superposition – in-plane moduli are within 3.3–7.5% relative error range.

In this paper, we investigate the applicability of two-step homogenization to the high-crimp woven composites. The paper is divided into two parts. In the first part, FEA is used to compare the effective elastic properties of an explicitly modeled sinusoidal-shape tow (fibers arranged in a hexagonal pattern embedded in isotropic matrix, see Fig. 1a) with the response obtained from homogenized wavy tows (Fig. 1b). Three sets of properties are considered in the latter case: micromechanical homogenization ([14,27]), and FEA homogenization of unidirectional composites with fibers embedded in isotropic matrix in square and hexagonal arrangements. The concept of a microscale periodic unit cell is utilized and periodic boundary conditions (PBC) are employed. In the second part of this paper, we present results of elastic homogenization for three configurations of 3D woven composites - 1×1 orthogonal, ply-to-ply and plain weave. The results are compared with experimental measurements and with a simple stiffness approximation approach (Voigt model) based on the effective stiffness matrices of wavy tows described in the first part of the paper.

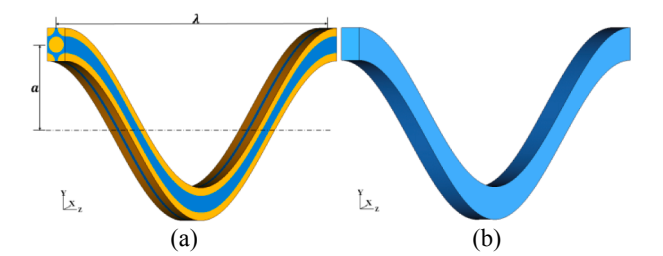


Fig. 1. (a) Amplitude a and wavelength λ shown on an explicit model; (b) homogenized model.

2. Geometry of tow paths in 3D woven composites

We analyzed tows of three woven architectures – 1×1 orthogonal, ply-to-ply and plain weave to determine the degree of waviness – crimp ratio defined as the ratio of amplitude to wavelength $CR = a/\lambda$, see Fig. 1a. Weave patterns and volume representations of all three architectures are shown in Fig. 2; tow and matrix volume fractions of each architecture are given in Table 1. The dimensions in the warp, weft, and thickness directions of the unit cells are: orthogonal $5.08 \times 5.08 \times 4.00 \text{ mm}^3$, plain weave – $5.08 \times 5.08 \times 3.90 \text{ mm}^3$, and ply-to-ply $-8.47 \times 8.47 \times 3.95 \,\mathrm{mm}^3$. In the orthogonal architecture, warp and weft tows do not interlace, however tows of the third type binder - go all the way through-thickness of the composite between weft tows. In the ply-to-ply architecture, tows from several layers interlace. On the other hand, in the plain weave architecture tows interlace within the same layer only. Geometry of the first architecture (Fig. 2a) was obtained from segmentation of X-ray computed microtomography data; geometries of the latter two were obtained from fabric mechanics simulations. Fully periodic final geometries of all three architectures were converted to finite element models, see Section 4.1 and [2] for details.

Crimp ratios of all tows in the architectures were calculated from tow centerlines. In [28], it is shown that wavy fiber tows can take different shapes, which affects how crimp is characterized. In the case of the three woven composite architectures discussed here, the tows fit two types shown in Fig. 3a and b. The orthogonal model is represented by the type shown in Fig. 3a, while the ply-to-ply and plain weave models are represented by the type shown in Fig. 3b.

In our analysis, crimp ratio of a tow is obtained by placing three target points on the tow's centerline. Based on the three points' "x" and "y" coordinates, the amplitude a and the wavelength λ of the quasisinusoidal shape are found and the crimp ratio is calculated. In Fig. 3, the three points are identified as "P1", "P2", and "P3". For the orthogonal model (type shown in Fig. 3a), the amplitudes are calculated from the differences between the "y" coordinates of points P1 and P2. The amplitudes of the plain weave and ply-to-ply models (type shown in Fig. 3b) are also found from the differences between the "y" coordinates of P1 and P2, but in this case, the difference is divided by two. Tow wavelengths are found from the differences between the "x" coordinates of points P1 and P3.

In the orthogonal configuration, the centerlines of the warp tows appear to be straight, however, local fiber waviness may be present, which can be seen indirectly in the varying thickness of the tows, see Fig. 4a. As will be shown in Section 5, even a small amount of waviness results in significant changes in the overall unit cell elastic properties. On the contrary, weft and binder tows present considerable waviness – crimp ratios of the weft tows fall in the range between 0.05 and 0.15 while the binder tows' crimp ratios (CR) are around 0.4. From the microtomography images, we estimated the normalized wavelength with respect to fiber diameter $d(\lambda/d)$ in the orthogonal configuration to be approximately 400 based on the highlighted weft tow shown in Fig. 4a (green). Fig. 4a (green) shows a weft tow with CR = 0.12, while Fig. 4a (blue) shows a binder tow with CR = 0.4. In the plain weave

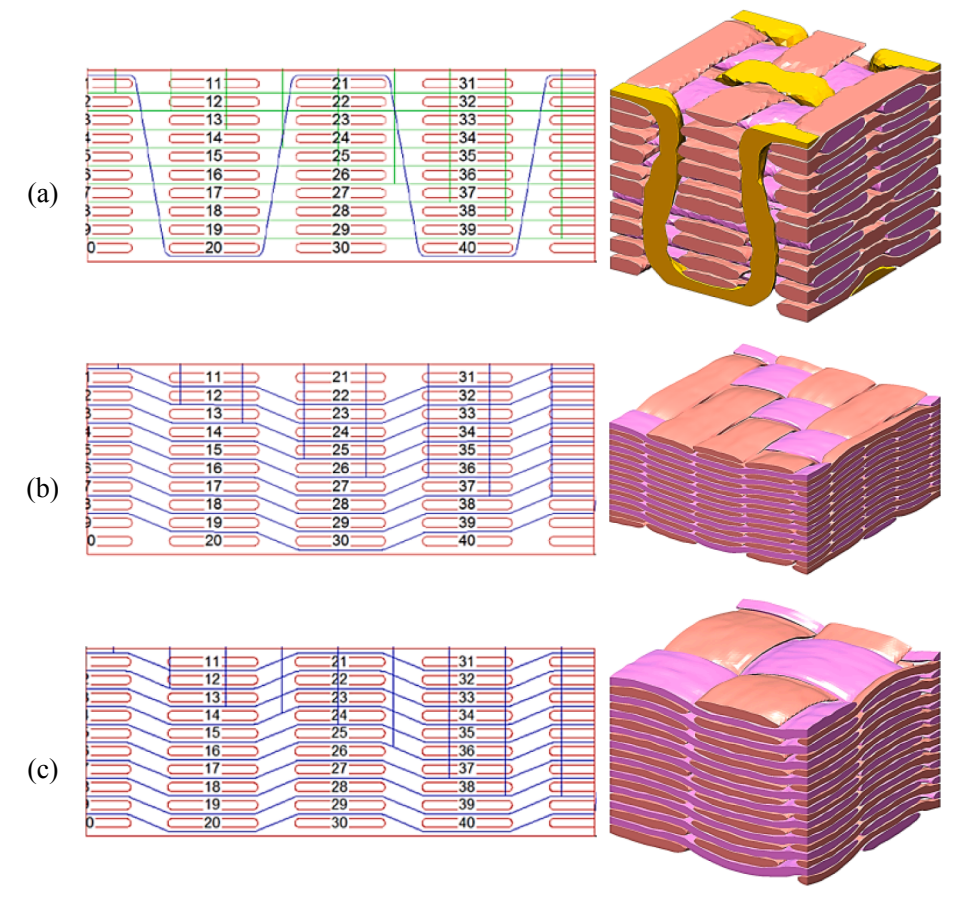


Fig. 2. Tow paths and final geometries of three architectures: (a) 1×1 orthogonal (b) ply-to-ply, (c) plain weave.

Table 1
Tow and matrix volume fractions (%) of the considered woven architectures.

Architecture	Warp	Weft	Binder	Matrix
1 × 1 Orthogonal	31.6	29.0	6.8	32.6
Ply-to-Ply	34.7	39.4	-	25.9
Plain Weave	39.7	36.2	-	24.1

architecture, the average crimp ratio value of 0.024 was found for weft and warp tows. Finally, in the ply-to-ply architecture, the average crimp ratio values of 0.026 and 0.025 were calculated for the weft and warp tows, correspondingly.

The method to estimate the crimp ratios of the warp and weft tows and the results are in agreement with work done by [29], where no large variation of crimp ratio was found among either warp or weft tows, meaning that a narrow range of *CR* can describe the in-plane tows of the composites discussed. Note that in this study we are not focusing on the variation of tow cross-sections throughout the unit cell. A detailed analysis of such variations in an orthogonal 3D woven composite can be found in [30].

3. Analysis of a wavy tow unit cell

Tow unit cells analyzed in this section are modeled to follow fiber paths which are assumed to have sinusoidal shapes (Fig. 1). In addition to crimp ratio (CR), wavelength normalized by fiber diameter (λ/d) is used as a parameter. In all of the models discussed, the fiber volume fraction is set to 70%.

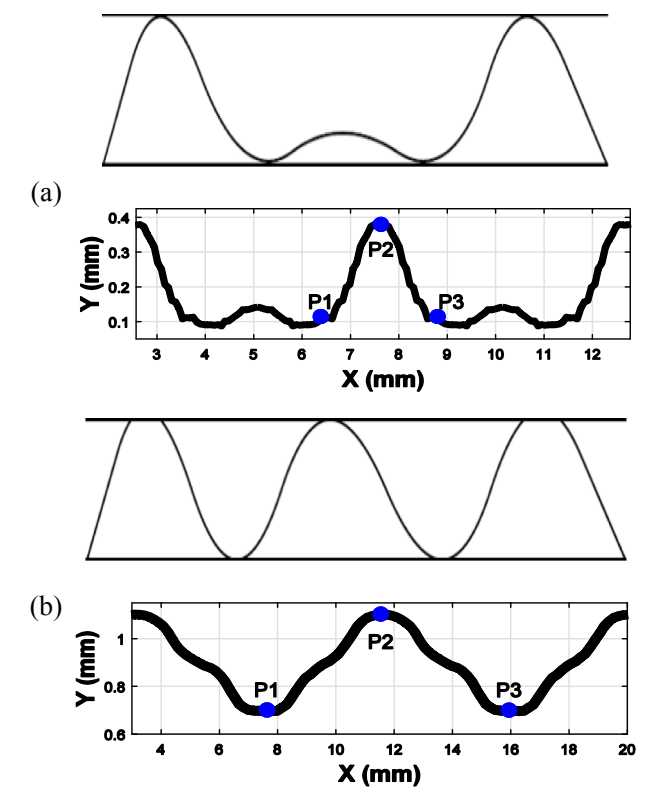


Fig. 3. Tow centerlines: (a) 1×1 orthogonal architecture; (b) ply-to-ply architecture.

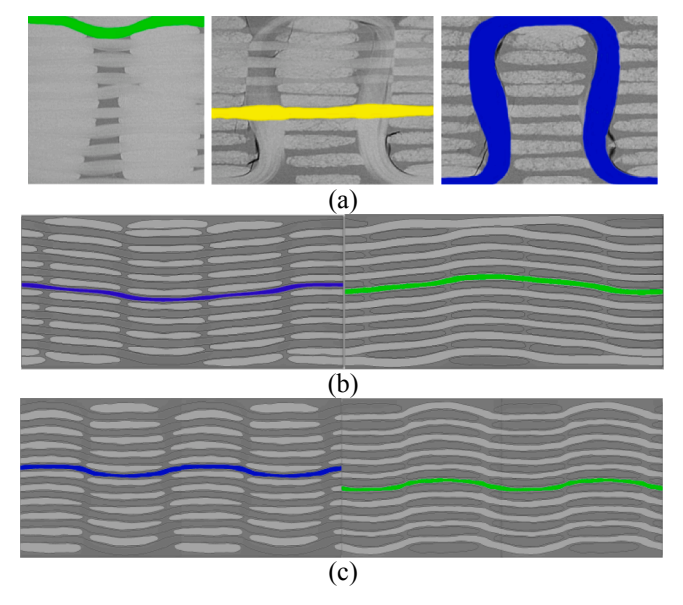


Fig. 4. Highlighted tows: (a) 1×1 orthogonal architecture data obtained from microtomography: weft (green), warp (yellow) and binder (blue): (b) ply-to-ply architecture obtained from digital fabric mechanics simulations: weft (green) and warp (blue); (c) plain weave obtained from digital fabric mechanics simulations: weft (green) and warp (blue).

3.1. Geometry and mesh generation

The final volume fraction is a function of the crimp ratio and initial fiber area fraction AF because area fraction of fibers changes throughout the tow path (see Fig. 5). For the final volume fraction VF = 70% and different crimp ratios, the choice of the initial AF is given in Table 2. As was discussed in Section 2, the majority of the tows within the analyzed woven composite architectures have crimp ratios within the range 0–0.15. In addition to crimp ratio, the normalized wavelength (λ/d) in this study is varied from 5 to 150. All values of the geometric parameters used are presented in Table 2. Note that binder tows are not considered due to their non-sinusoidal shape – in order to use the appropriate PBCs, the geometry of the tow unit cell has to be periodic in all three directions, which is not observed in the throughthickness direction of the binder tow, see Fig. 4a.

The geometry and mesh generation procedure that follows is based on [31–33]. Using a custom MATLAB script, the "first" cross section (see "1" in Fig. 5) is generated and meshed MSC Marc Mentat with four-node quadrilateral elements. It is then duplicated along a sinusoidal curve of a given *CR* to generate 3D FEA mesh. Fiber cross-sections at minima and maxima of the centerline path have circular shapes, while all others are represented by ellipses, see Fig. 5. To achieve this, fiber cross-sections at these locations must be deformed during geometry generation, which distorts the surrounding matrix mesh (see 2 in

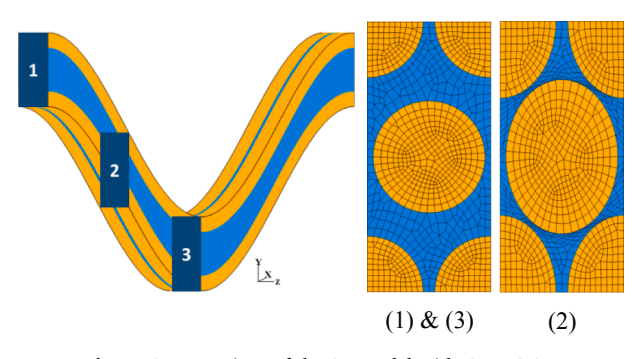


Fig. 5. Cross sections of the 3D model with CR = 0.15.

 Table 2

 Geometric parameters of the considered wavy tow unit cell models.

CR	λ/d	d	AF	VF
0.05	5, 10, 20, 50, 100, 150	0.8690	68.5%	70.0%
0.10	5, 10, 20, 50, 100, 150	0.8416	64.2%	70.0%
0.15	5, 10, 20, 50, 100, 150	0.8054	58.8%	70.0%

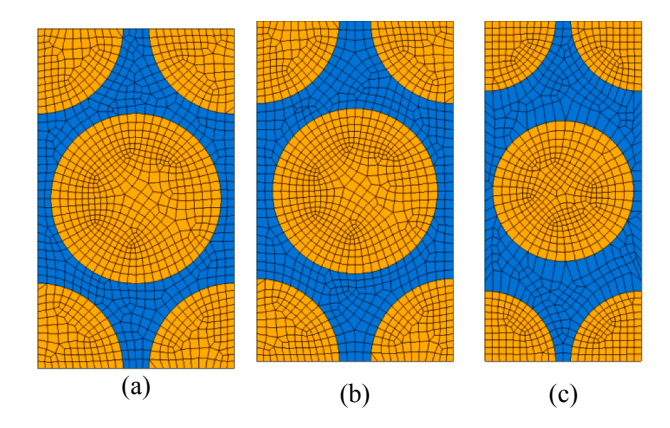


Fig. 6. Cross sections used to generate 3D models: (a) CR = 0.05; (b) CR = 0.10; (c) CR = 0.15.

Fig. 5). To eliminate mesh overlapping, Taubin's relaxation [34] is applied to the matrix elements. The final mesh is free of geometric incompatibilities; perfect bonding between the matrix and the fibers is assumed.

The standard value for the height to width ratio of a unit cell with hexagonal packing $(\sqrt{3})$ is used to create the cross sections for the models with CR = 0.05 and 0.10 (Fig. 6a and b). At this ratio, the final VF = 70% is achieved without mesh overlapping. On the other hand, for the highly crimped tow (CR = 0.15) the overlapping could not be avoided with the same ratio. Therefore, a modified cross section ratio of 2.19 is used for the model with CR = 0.15 to avoid mesh overlapping (Fig. 6c). This modification gives rise to an orthotropic rather than a transversely isotropic behavior obtained from the other cross sections (Fig. 6a and b), which may affect the predictions of the macroscopic effective properties at CR = 0.15.

3.2. Material properties

In the explicit tow unit cell (Fig. 1a) and unidirectional models (Fig. 7), transversely isotropic properties of IM7 carbon fiber and isotropic properties of RTM6 resin are used. For the homogenized model (Fig. 1b) the effective material properties obtained from tow homogenization via micromechanical formulas presented in [35], and FEA of

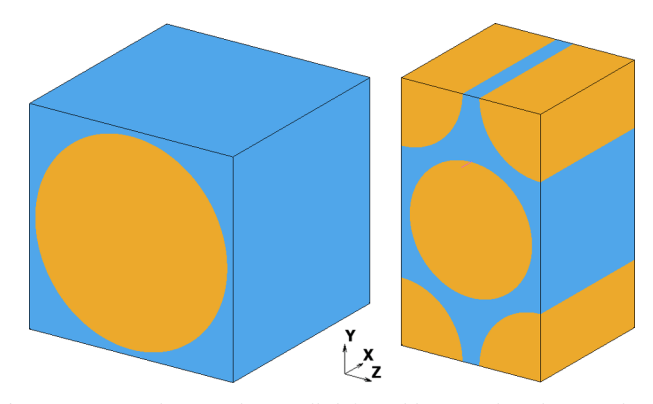


Fig. 7. Square unidirectional unit cell (left) and hexagonal unidirectional unit cell (right).

Table 3Elastic properties of the constituents and homogenized properties of unidirectional tows.

	Constituents			Homogenized	
	Carbon IM7	Epoxy RTM6	Analytical [35]	FEA Square	FEA Hexagonal
E _L (GPa)	276.0	2.890	194.1	194.0	194.0
E_T (GPa)	23.10	_	10.71	11.88	10.23
$ u_{LT}$	0.3500	0.3500	0.3500	0.3501	0.3501
$ u_{TT}$	0.3000	_	0.3638	0.3218	0.3942
G_{LT} (GPa)	27.60	1.070	5.007	5.976	5.095
G_{TT} (GPa)	8.885	_	3.926	3.165	3.671

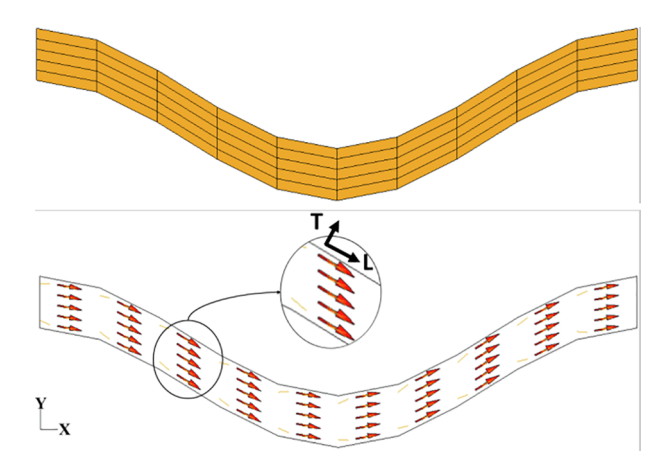


Fig. 8. Local material orientations in a 3D unit cell (coarse mesh).

square and hexagonal fiber arrangements (Fig. 7) are used. Note that the square fiber arrangement does not exhibit the transverse isotropy observed for hexagonal arrangements.

All material properties used are summarized in Table 3. Transversely isotropic properties denoted by 'L' and 'T' correspond to the longitudinal and transverse fiber directions, correspondingly. Local material orientations in the FEA models are assigned to each element via the previously described geometry generation MATLAB script (see Section 3.1). Fig. 8 illustrates local material orientations in the homogenized model. For both square and hexagonal packing geometries, direction 'T' is parallel to the y-axis.

3.3. Boundary conditions

Periodic boundary conditions (PBCs) can be used to represent a tow containing thousands of fibers using a single unit cell, see [31–33], and [11] for other applications of PBCs. Use of PBCs helps reduce the required computational resources and enables quick parametric studies. In our models, PBCs are implemented using the "servo-link" feature of MSC Marc Mentat. The periodicity conditions for two nodes on opposite faces of a unit cell are

$$\mathbf{u}_{x_i+} - \mathbf{u}_{x_i-} = \delta_{x_i} \qquad (i = 1, 2, 3)$$
 (1)

where $\mathbf{u}_{x_i^+}$ and $\mathbf{u}_{x_i^-}$ are displacement vectors of two nodes on the positive and negative x_i faces of a unit cell, respectively, and δ_{x_i} is the average displacement applied between the faces. Fig. 9a shows PBCs for the corner nodes of the considered tow unit cell model – other links are hidden

In order to obtain the stress components needed for calculating effective properties of a tow unit cell, six load cases are analyzed: (1) tension in "x", (2) tension in "y", (3) tension in "z", (4) shear in "x-y" plane, (5) shear in "y-z" plane, and (6) shear in "x-z" plane. Fig. 9 shows distribution of the stress component σ_{xx} (MPa) in the unit cell with CR=0.10 and $\lambda/d=20$ with material properties given in Table 3, under load case (1) for the applied strain $\varepsilon_{xx}=0.001$.

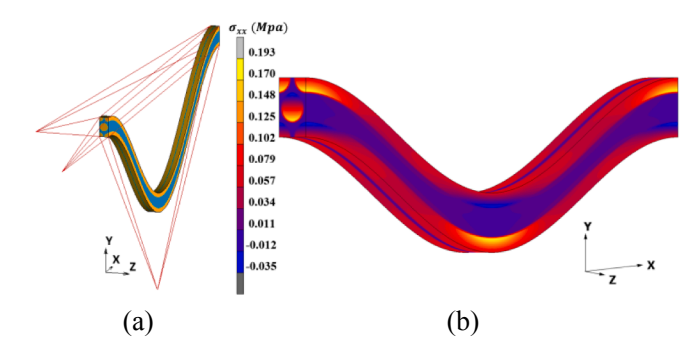


Fig. 9. Wavy unit cells: (a) periodic boundary conditions; (b) distribution of the stress component σ_{xx} in the explicit model with CR = 0.10 and $\lambda/d = 20$.

3.4. Processing of the results

Processing of the FEA simulation results follows the procedure previously described in [36,37]. Volume averaging of stress and strain components is carried out to estimate the effective elastic properties of each unit cell in this work. The same procedure is used to process data from tow and woven unit cells. Unit cell volume averages of stress components are found as:

$$\langle \sigma_{ij} \rangle_k = \frac{1}{V} \sum_l (\sigma_{ij}^{(l)})_k \nu^{(l)}, \qquad (i, j = 1, 2, 3)$$
 (2)

where the load case number k ranges from 1 to 6, corresponding to the three tensile (1,2,3) and three shear (4,5,6) load cases, $\langle \sigma_{ij} \rangle_k$ is the volume average of the stress component ij calculated from the k-th load case, $(\sigma_{ij}^{(l)})_k$ is the stress component ij at the centroid of the element l calculated from the k-th load case, V is the total volume of the unit cell, and $\nu^{(l)}$ is the volume of the finite element number l. Given all volume-averaged stress components and applied strains, the effective stiffness matrix \mathbf{C} is calculated [32]. The compliance matrix \mathbf{S} is found as the inverse of \mathbf{C} , and the engineering elastic constants are computed as $E_k = 1/S_{kk}$ where k = 1, 2, and 3, $\nu_{12} = -S_{21} \cdot E_1$, $\nu_{23} = -S_{32} \cdot E_2$, $\nu_{13} = -S_{31} \cdot E_1$, $G_{12} = 1/2S_{66}$, $G_{23} = 1/2S_{44}$, $G_{31} = 1/2S_{55}$.

3.5. Validation of the FEA approach

We validated our FEA approach for a tow unit cell by comparing with the results published in [11]. In that work, the authors applied the same six load cases as described in Section 3.3 to sinusoidal tows with VF of 70% and normalized wavelength of 20. The fiber is considered to be transversely isotropic with material properties of $E_L = 207.5$ GPa, $E_T = 25$ GPa, $\nu_L = 0.24$, $\nu_T = 0.359$, $G_L = 95$ GPa and $G_T = 9.2$ GPa. The matrix is isotropic with E = 4.5 GPa and V = 0.34. We investigate three values of the crimp ratio: CR = 0, 0.05, and 0.10.

We consider two models: in the first, "scaled" model, cross-sections are locally scaled to preserve circularity of the fibers, see Fig. 5; in the second, "adapted" model, cross-sections are duplicated along the entire tow path without local scaling, see cross-section 1 in Fig. 5. Note that the "adapted" model is assumed to follow the geometry generation

Table 4
Comparison of effective elastic properties of explicitly modeled wavy tow unit cells: "scaled" model vs results from [11].

	CR	E_{x}	E_y	$E_{\mathcal{Z}}$	$G_{\chi y}$	$G_{\chi\chi}$	G_{yz}	ν_{xy}	$ u_{xz}$	ν_{yz}
"Scaled" [11]	0	146.6 145.7	13.39 13.35	13.39 13.34	8.863 8.649	8.862 8.715	4.760 4.712	0.266 0.266	0.266 0.266	0.408 0.405
Difference, %		0.6	0.3	0.4	2.5	1.7	1.0	0	0	0.6
"Scaled"	0.05	95.07	13.87	13.28	9.647	8.551	4.924	0.244	0.294	0.407
[11]		91.24	13.71	13.35	9.160	8.602	4.829	0.260	0.283	0.399
Difference, %		4.2	1.2	-0.5	5.3	-0.6	2.0	-6.1	3.8	2.0
"Scaled"	0.10	59.00	15.81	13.05	11.36	8.120	5.363	0.138	0.367	0.419
[11]		48.38	14.94	13.40	10.41	8.252	5.203	0.239	0.304	0.384
Difference, %		22	5.8	-2.6	9.1	-1.6	3.1	-42	21	9.2

procedure presented in [11] and is introduced only for comparison with the previously published result. The resulting fiber volume fraction in both models was set to 70%. As a result, the area fraction AF at maxima is 64.24% for "scaled" model and 70% for "adapted".

The effective Young's moduli, shear moduli and Poisson's ratios of the "scaled" model are compared with results from [11] for different crimp ratios in Table 4; the comparison of the "adapted" model results with [11] is given in Table 5. For CR = 0 (straight fiber) the results from both models and [11] are all in good agreement – the minor error is assumed to be numerical. As the crimp ratio is increased to 0.05 and further to 0.10, "scaled" and "adapted" models give different predictions. The relative error in the longitudinal Young's moduli between the "scaled" model and [11] is 22%, while between the "adapted" model and [11] the error is only 3.3%. Relative errors between the remaining Young's and shear moduli are not as pronounced – the average errors are 4.4% and 1.7% in the cases of the "scaled" and the "adapted" models, correspondingly.

Few details on geometry and mesh generation are provided in [11], but from the comparison it appears that the authors did not apply local fiber scaling, which means the circularity of the fiber is not preserved. It also appears that even in the case of moderate waviness, i.e. CR=0.10, local fiber scaling has a significant effect on the longitudinal Young's modulus and thus cannot be neglected. We also conclude that given the same geometry our FEA procedure yields similar results compared with the procedure previously published in [11].

3.6. Results

The effective Young's moduli E_x , E_y and E_z , shear moduli G_{xy} , G_{yz} and G_{xz} , and Poisson's ratios v_{xy} , v_{yz} , and v_{xz} are presented in this section for the set of explicit and homogenized models with geometric parameters given in Table 2.

Note that the "Analytical", "Hexagonal", and "Square" models discussed in this section are based on the homogenized tow properties obtained from analytical formulas [35] and FEA homogenization of hexagonal and square unidirectional unit cells. Table 3 presents

properties of the composite constituents and homogenized properties of the tows, and Fig. 7 illustrates the unidirectional tow unit cells.

3.6.1. Young's moduli

A comparison of the Young's modulus E_x predicted by each of the three homogenized FEA models and the explicit FEA model is shown in Fig. 10 for $CR=0.05,\,0.10,\,$ and 0.15. As can be seen from the results of the explicit model, E_x decreases to an asymptotic value as the normalized wavelength λ/d increases – the transition occurs around $\lambda/d=50$. It appears that the explicit model's values at $\lambda/d=50$ and $\lambda/d=150$ can be considered the same. The differences between these values are 1.1%, 1.5%, and 2.6% for crimp ratios 0.05, 0.10, and 0.15, respectively. Therefore, it can be said that "infinitely" long fiber predictions are obtained at $\lambda/d=50$. Note that the presented three homogenized models' results do not depend on λ/d because fiber diameter does not affect the homogenization results in the case of a unidirectional composite, which is how the properties were calculated for the homogenized analytical, square and hexagonal models shown.

As the CR increases E_x value decreases as predicted by all models. The homogenized analytical and hexagonal models are virtually the same (relative differences are equal to 0.9% at CR = 0.05, 0.8% at CR = 0.10, and 0.3% at CR = 0.15). The homogenized square model, when compared to the hexagonal model, shows consistently higher predictions with the difference of 10.5%, 14.2%, and 15.1% for CR = 0.05, 0.10, and 0.15, respectively. This may be attributed to the non-isotropic transverse response of the square arrangement.

Explicit model predictions converge to different homogenized models at different crimp ratios. At CR=0.05, the explicit model approaches the homogenized hexagonal (analytical) model (4.5% higher than the hexagonal, $\lambda/d=50$). On the other hand, at CR=0.10 and 0.15, the explicit model approaches the square model predictions – 2.07% higher than the square (CR=0.10 and $\lambda/d=50$), and 0.14% higher than square (CR=0.15 and $\lambda/d=50$). Note that in the previously discussed study [11], the dependence of the overall tow properties on the normalized wavelength λ/d is not investigated.

Similarly to E_x , Young's modulus E_y decreases to an asymptotic

Table 5 Comparison of effective elastic properties of explicitly modeled wavy tow unit cells: "adapted" model vs results from [11].

	CR	E_{x}	E_y	$E_{\mathcal{Z}}$	G_{xy}	$G_{\chi\chi}$	G_{yz}	ν_{xy}	$ u_{\chi\chi}$	$ u_{yz}$
"Adapted"	0	146.6	13.39	13.39	8.863	8.862	4.760	0.266	0.266	0.408
[11]		145.7	13.35	13.34	8.649	8.715	4.712	0.266	0.266	0.405
Difference, %		0.6	0.3	0.4	2.5	1.7	1.0	0	0	0.6
"Adapted"	0.05	92.42	13.74	13.40	9.382	8.750	4.875	0.261	0.284	0.401
[11]		91.24	13.71	13.35	9.160	8.602	4.829	0.260	0.283	0.399
Difference, %		1.3	0.2	0.3	2.4	1.7	1.0	0.5	0.3	0.4
"Adapted"	0.10	49.99	14.73	13.44	10.76	8.496	5.188	0.256	0.299	0.385
[11]		48.38	14.94	13.40	10.41	8.252	5.203	0.239	0.304	0.384
Difference, %		3.3	-1.4	0.3	3.3	3.0	-0.3	7.0	-1.7	0.1

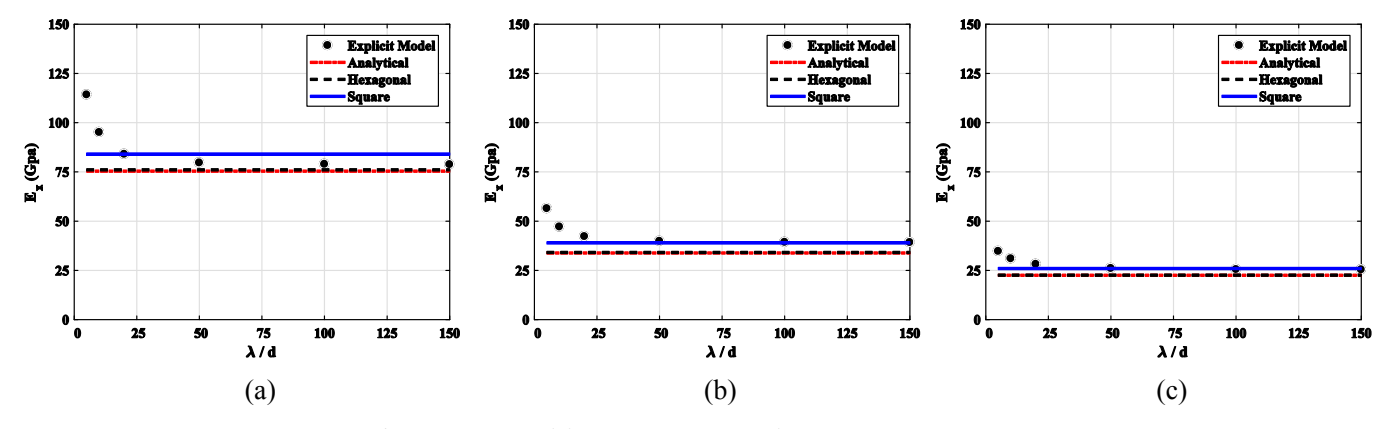


Fig. 10. Young's modulus E_x : (a) CR = 0.05; (b) CR = 0.10; (c) CR = 0.15.

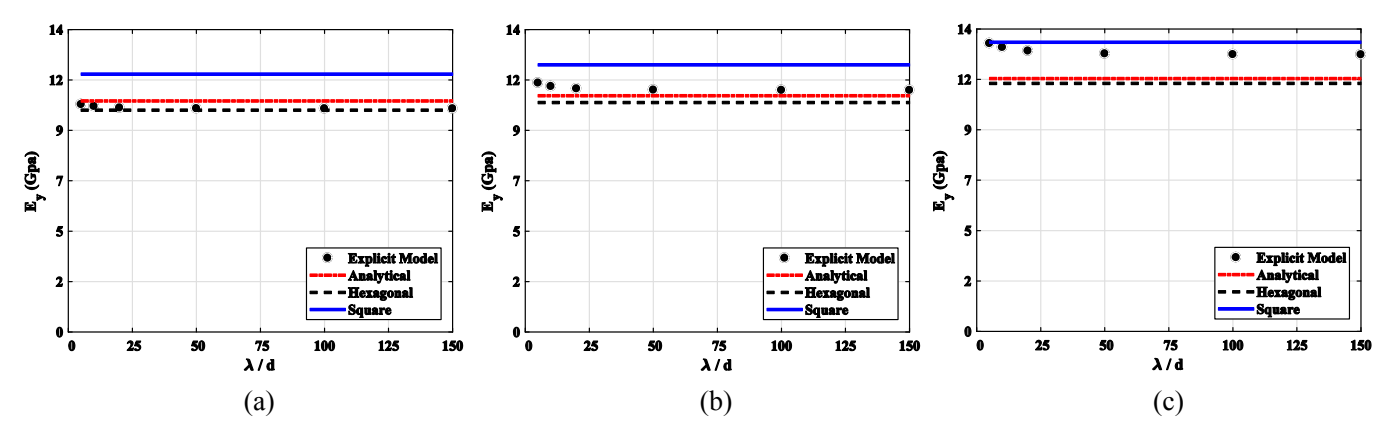


Fig. 11. Young's modulus E_y : (a) CR = 0.05; (b) CR = 0.10; (c) CR = 0.15.

value as the normalized wavelength increases, with separation of scales attained again at $\lambda/d=50$, see Fig. 11. The predicted values of all models increase as CR increases, which is opposite to E_x behavior. Another contrast is the sensitivity to the normalized wavelength λ/d , while the sensitivity of E_x appears to decrease, the sensitivity to λ/d of E_y increases as CR increases. The explicit FEA model converges to the hexagonal model's prediction at CR=0.05 (difference of 0.7%), at CR=0.10 it converges to the analytical model's prediction (difference of 2.3%), and at CR=0.15 the explicit model converges to the square model's value (difference of -4.5%). It also appears that the difference between homogenized analytical and hexagonal models decreases as the crimp ratio increases – the analytical is higher than the hexagonal by 4.1% at CR=0.05, 3.0% at CR=0.10, and 1.9% at CR=0.15. Again, homogenized square model presents the highest predictions among all crimp ratios.

Young's modulus in the third direction (E_z) does not appear to be significantly affected by either CR or λ/d (see Fig. 12). The homogenized hexagonal model gives the best estimate for E_z predictions compared with the explicit model at crimp ratios CR = 0.05 and CR = 0.10 (the maximum relative error is 4.19% at $\lambda/d = 50$). For the crimp ratio 0.15, the analytical model is the closest to the explicit model (relative error of -2.07% at $\lambda/d = 50$). In agreement with E_x and E_y results, the homogenized square model's predictions for E_z are higher than any other homogenized model predictions discussed here.

3.6.2. Shear moduli

Fig. 13 presents the results for the effective shear modulus G_{xy} obtained from the explicit and homogenized models. At the lowest crimp ratio (CR = 0.05), sensitivity to λ/d is not observed. For higher values of crimp ratio, the increases with the crimp ratio (see Fig. 13b and c). As

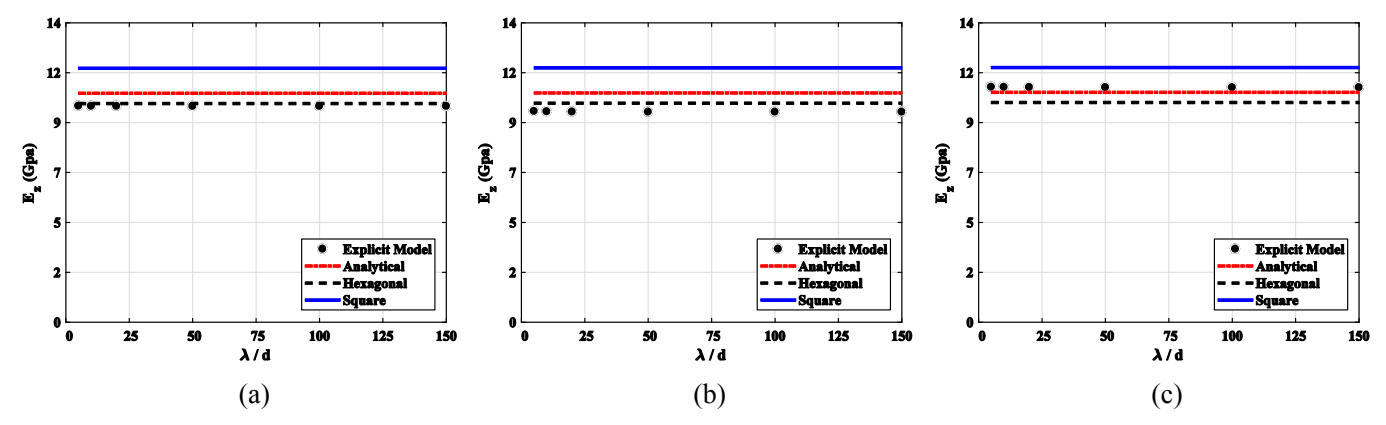


Fig. 12. Young's modulus E_z : (a) CR = 0.05; (b) CR = 0.10; (c) CR = 0.15.

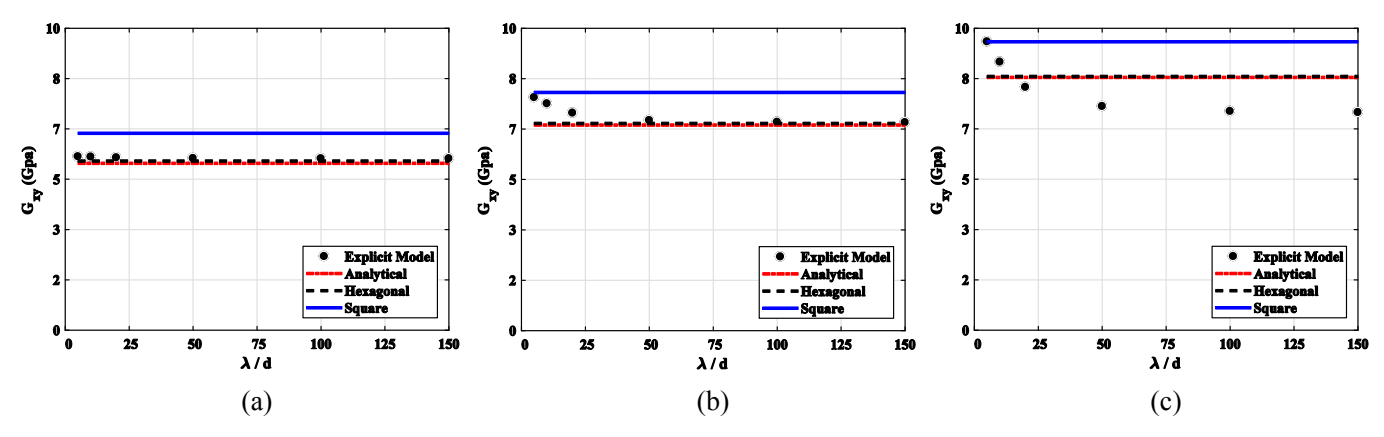


Fig. 13. Shear modulus G_{xy} : (a) CR = 0.05; (b) CR = 0.10; (c) CR = 0.15.

was previously seen in the results for E_x , homogenized analytical and homogenized hexagonal predictions are almost the same (maximum relative error is 1.4% at CR=0.05 and $\lambda/d=50$). At crimp ratios 0.05 and 0.10, the explicit model converges to the hexagonal/analytical predictions, while at CR=0.15 there is no convergence between the explicit model and any homogenized model, and the explicit model's asymptotic value is considerably lower than the lowest homogenized model's predictions. Homogenized square model's predictions present the highest values at all studied crimp ratios. In the cases CR=0.10 and CR=0.15, separation of scales happens at $\lambda/d=50$.

Similarly to the Young's modulus E_x and shear modulus G_{xy} , the homogenized hexagonal predictions and the homogenized analytical predictions for G_{yz} are similar (maximum relative error of 6.23%, see Fig. 14a with $\lambda/d=50$). With respect to the explicit model results, there is no considerable sensitivity to the normalized wavelength for any of the three crimp ratios discussed, and the values predicted by this model are between the values from homogenized analytical (upper bound) and homogenized hexagonal (lower bound). In addition, the asymptotic value of G_{yz} (explicit model) increases with crimp ratio. In contrast to the previous results in this section, the homogenized square results are the lowest among all predictions.

Fig. 15 shows the predictions for G_{xz} . The dependence of the explicit model's predictions on the normalized wavelength λ/d appears to increase with crimp ratio, however, it remains virtually negligible in the considered range of CR. As the crimp ratio increases, all homogenized predictions decrease slightly. At lower crimp ratio values, 0.05 and 0.10, the explicit model's predictions converge to the homogenized analytical/hexagonal values (see Fig. 15a and b), presenting the same trend observed in Fig. 13a and b, for G_{xy} . At CR = 0.15 the explicit model converges to the homogenized square FEA, and, in comparison to other previously discussed results, this behavior is also seen for E_x (CR = 0.10 and 0.15), and E_y (CR = 0.15). Similarly to the

previously discussed E_x , E_y , E_z and G_{xy} , homogenized analytical and homogenized hexagonal predictions are the same and the homogenized square predictions have the highest values among all homogenized models.

3.6.3. Poisson's ratios

The explicit model's predictions of Poisson's ratio in the longitudinal direction, ν_{xy} , increase with λ/d and decrease with CR, see Fig. 16. As can be seen in Fig. 16, the asymptotic values are reached at normalized wavelength $\lambda/d=50$. There is almost no agreement between the explicit model and the homogenized models because the only convergence is seen at CR=0.05 between the homogenized square and explicit model (see Fig. 16a).

All predictions for ν_{yz} decrease as crimp ratio increases, see Fig. 17. Furthermore, the explicit model's predictions do not exhibit as high dependence on the normalized wavelength as in the case of ν_{xy} , and again the asymptotic values are reached around $\lambda/d=50$. Homogenized hexagonal model is the only one that appears to predict the explicit model's results well, and only at CR=0.05 and 0.15.

Results for Poisson's ratio ν_{xz} are presented in Fig. 18. The explicit model's results exhibit higher sensitivity to the normalized wavelength than ν_{yz} , but lower than ν_{xy} . The asymptotic values are reached at the same normalized wavelength $\lambda/d=50$. As it was determined for ν_{yz} , results of the explicit FEA are close to the homogenized hexagonal predictions at crimp ratios CR=0.05 and 0.15 while being very different from all homogenized models at CR=0.10. Overall, the explicit model's asymptotic values exhibit minor dependence on CR.

4. Analysis of woven composite unit cells

The results of Section 3 indicate that the two-step homogenization approach in which tows are modeled as solid objects with homogenized

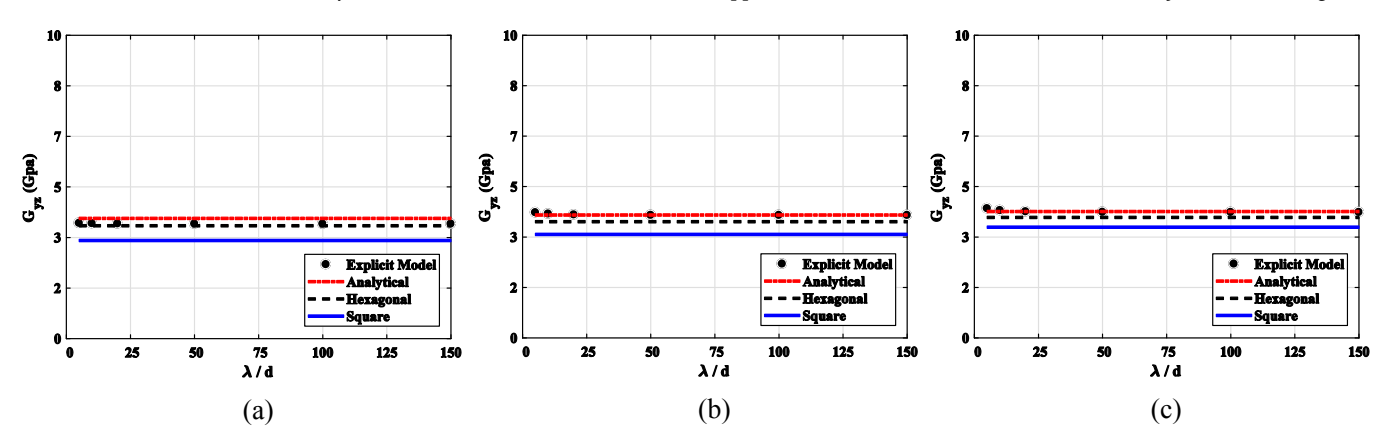


Fig. 14. Shear modulus G_{yz} : (a) CR = 0.05; (b) CR = 0.10 (c) CR = 0.15.

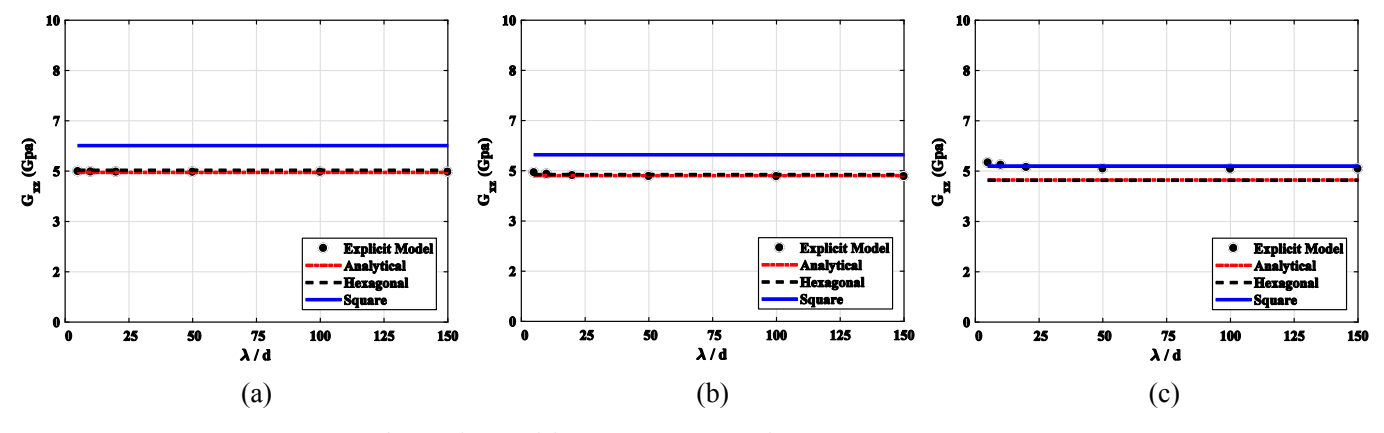


Fig. 15. Shear modulus G_{xz} : (a) CR = 0.05; (b) CR = 0.10; (c) CR = 0.15.

properties may be applicable to high-crimp woven composites if the ratio of fiber wavelength to its diameter (λ/d) is high. In the case of the explicit model asymptotic values are reached around $\lambda/d=50$ and the actual ratio calculated from microscopy is around 400 (see Section 2). For most of the engineering constants, the model based on analytical homogenization appears to correlate well with the explicit model's results.

In this section, the second step of the two-step homogenization procedure is performed – overall elastic properties of meso-scale 3D woven composite unit cells are found. Two approaches are utilized: direct FEA analysis and and Voigt approximation.

4.1. Direct FEA

Two methods were used to create three-dimensional meshes of the considered 3D woven composites: fabric mechanics simulations and microtomography data processing. Fabric mechanics simulations were performed in DFMA (Digital Fabric Mechanics Analyzer, see [38–40]). The second method consisted of processing microtomography images of a sample with orthogonal woven architecture in ImageJ [41]. The images were segmented into individual tows which were then exported in STL format. The tows were meshed in MSC Patran and assigned material orientations following tow centerlines.

The first method (DFMA) was used to obtain the ply-to-ply and the plain weave models, and the second method (μ CT) was used to obtain the 1 \times 1 orthogonal model. Detailed description of the architectures' tow geometries is given in Section 2, and the final reinforcement geometries are shown in Fig. 2. Tows in all three models were assigned the homogenized "analytical" material properties given in Table 3. Fiber volume fraction of 70% was used. Periodic boundary conditions were used, and each model was subjected to six load cases: three uniaxial tension and three shear cases. All boundary conditions and load cases

are the same as discussed in Section 3.3 with applied strain of 0.001.

Detailed description of the geometry processing, meshing and FEA model preparation of these and similar models can be found in [2,35,42].

4.2. Stiffness approximation

The homogenization applied to the wavy unit cells in Section 3 results in a set of nine independent stiffness components (C_{ij} where i, j = 1...6). We used these C_{ij} values to estimate the overall properties of 3D woven composite unit cells with wavy tows. We selected the data at normalized wavelength $\lambda/d = 50$ for the models with crimp ratio CR = 0.05, 0.10 and 0.15. (see Appendix A). For any value between these crimp ratios a linear interpolation was used to estimate the stiffness matrix components.

After determining the overall stiffness values of individual wavy tows, the effective stiffness matrix C_{ij} of the 3D woven composite unit cell was estimated from the Voigt model based on the stiffness matrices $C_{ij}^{(k)}$ of the contributing wavy tows and the matrix:

$$C_{ij} = \frac{1}{V} \sum_{k=0}^{n} C_{ij}^{(k)} v^{(k)} \qquad (i, j = 1, ...6)$$
(3)

where n is the total number of tows in the architecture, V is the total volume of the unit cell, and $v^{(k)}$ is the volume of the k-th tow (k > 0) or the matrix (k = 0). The effective engineering constants are then found from the stiffness matrix components, see Section 3.4.

In this work, the stiffness values used for binder tows were the same as for sinusoidal tows with CR = 0.15 because periodic wavy tow unit cells cannot be generated for the actual binder tow crimp ratios (CR = 0.4) with the current procedure.

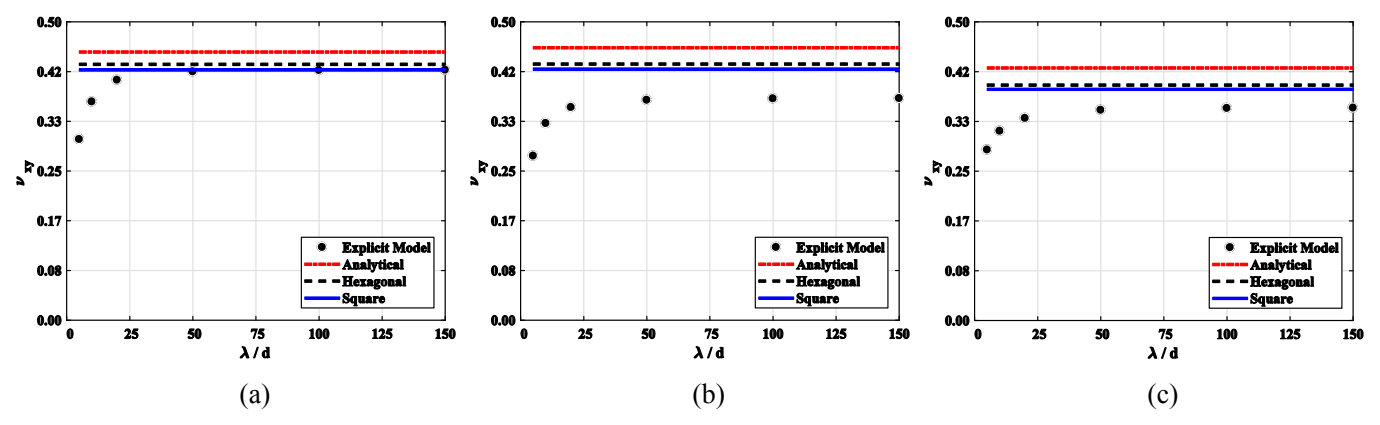


Fig. 16. Poisson's ratio v_{xy} : (a) CR = 0.05; (b) CR = 0.10; (c) CR = 0.15.

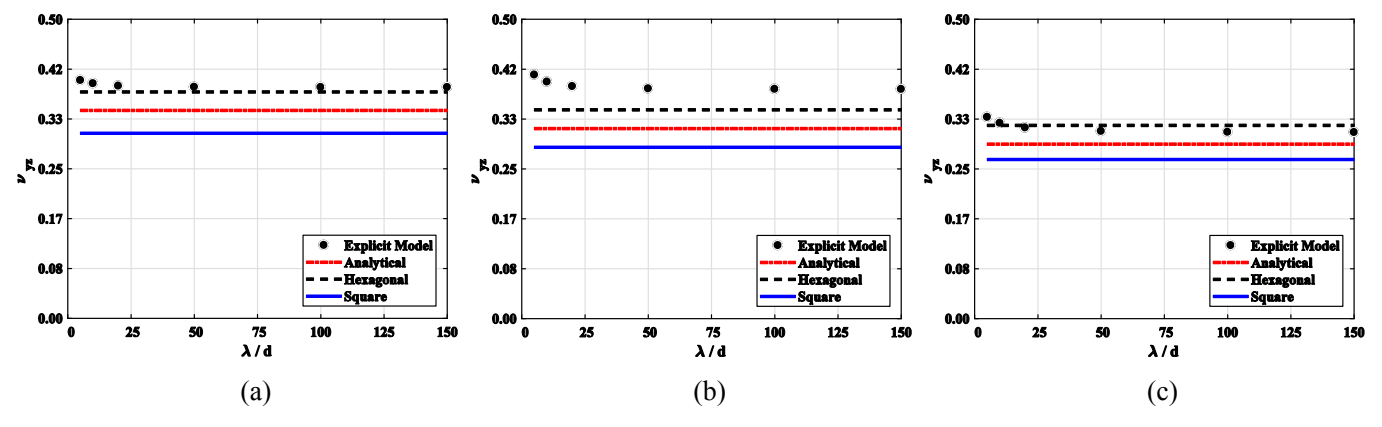


Fig. 17. Poisson's ratio v_{VZ} : (a) CR = 0.05; (b) CR = 0.10; (c) CR = 0.15.

4.3. Results

The effective engineering constants of the considered 3D woven composite unit cells calculated using the direct FEA and the stiffness approximation procedures are presented in Table 6. The results indicate that the approximation approach may be used as the first-order approximation of Young's moduli of low-crimp architectures such as plain weave or ply-to-ply. The calculated errors are in the range of 6–17% with the through-thickness modulus being overestimated by the approximation, and the in-plane moduli – underestimated. Young's moduli of the considered high-crimp architecture (orthogonal) are greatly underestimated – the calculated errors are in the range of 16–31%. As expected, the approximation does not work for Poisson's ratios or shear moduli.

The approximation does not account for the shapes of tow cross sections and interaction between tows. In addition, it depends on the accurate estimation of crimp ratios of tows – as it is shown, for example, in Fig. 10, the stiffness values are highly sensitive to CR values; hence, underestimation of CR leads to overestimation of stiffness and viceversa. It appears that the values of CR might be overestimated in all three models since the Young's moduli E_1 are underestimated (see Fig. 10). The overprediction of G_{12} by the approximation method is another indicator that the CR was overestimated in all three models (see Fig. 13).

Experimental measurements for the in-plane Young's moduli of the orthogonal architecture were performed by [43]. The average values are: $E_1 = 77.27$ GPa and $E_2 = 65.76$ GPa. It is clear that the two-step homogenization based on segmentation of the microtomography data provides good correlation with averaged experimental results having less than 10% of relative difference ($\delta E_1 = -6.3\%$, and $\delta E_2 = -7.1\%$). Considering the full range of the measured moduli (see [43]), the FEA results are within the in-plane results ($E_1 = 72.3...84.12$ GPa, and

Table 6Estimated effective elastic properties based on the direct finite element analysis and the stiffness approximation.

	Orthog	onal		Plain v	veave		Ply-to-ply			
	FEA	Appr.	%	FEA	Appr.	%	FEA	Appr.	%	
E ₁ (GPa)	73.44	61.86	-16	60.86	57.06	-6.2	59.77	53.03	-11	
E_2 (GPa)	62.99	43.30	-31	62.65	57.76	-7.8	69.55	57.75	-17	
E_3 (GPa)	11.97	9.138	-24	8.833	9.733	10	9.028	9.592	6.2	
ν_{12}	0.055	0.070	29	0.101	0.057	-43	0.079	0.057	-28	
ν_{23}	0.333	0.423	27	0.494	0.423	-14	0.490	0.423	-14	
ν_{13}	0.397	0.427	7.4	0.462	0.423	-8.4	0.450	0.423	-6.1	
G_{12} (GPa)	4.412	5.246	19	3.749	5.208	39	3.836	5.203	36	
G ₂₃ (GPa)	2.952	4.415	50	2.937	4.446	51	3.031	4.475	48	
G ₃₁ (GPa)	2.986	4.547	52	2.943	4.437	51	2.991	4.416	48	

 $E_2 = 60.8...70.78$ GPa).

5. Conclusions

In this paper, we examined applicability of the two-step elastic homogenization approach to 3D woven composite materials with high crimp ratios and presented the results of the numerical homogenization for three architectures: orthogonal, ply-to-ply and plain weave.

In the first part of the paper (Section 3), we focus on the elastic responses of individual fiber-reinforced tows having sinusoidal paths as functions of "waviness" (crimp ratio CR) and wavelength normalized with respect to the fiber diameter (λ/d). The range of CR values was determined from geometry analysis of the three available architectures. Each tow in our analysis was represented by a curvilinear unit cell subjected to periodic boundary conditions. The tows were modeled as homogeneous and explicit. In the homogeneous case, the overall

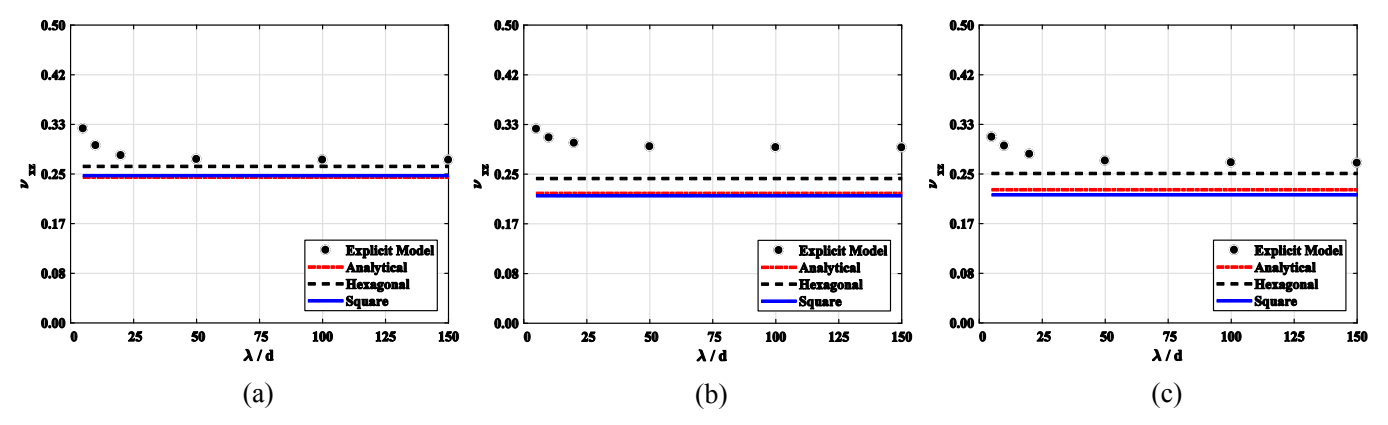


Fig. 18. Poisson's ratio v_{xz} : (a) CR = 0.05; (b) CR = 0.10; (c) CR = 0.15.

properties calculated from analytical homogenization and FEA of unidirectional unit cells (square and hexagonal) were applied to the entire unit cell. In the explicit case, fibers were modeled explicitly with five fibers per unit cell in hexagonal arrangement.

Tow unit cell results are presented as plots of each of the nine orthotropic engineering constants versus normalized wavelength for several values of crimp ratio. From the results of the "explicit" models, it was observed that moduli E_x , E_y and G_{xy} decrease with increasing λ/d while E_z , G_{yz} and G_{zx} do not exhibit significant dependence on λ/d . All moduli predictions reach their asymptotic values around $\lambda/d=50$, at which point we assume separation of scales – unit cell length is much larger than the fiber diameter therefore the fiber can be approximated as infinitely long. In this case, the elastic response depends on crimp ratio alone. From the optical microscopy analysis, it was determined that in the considered 3D carbon fiber/epoxy matrix composites, the actual normalized wavelength values are significantly greater than the threshold value of 50 (see Section 2). This means that the separation of scales required for two-step homogenization can be safely assumed for these composites.

Predictions from the homogenized unit cells do not depend on the λ/d parameter because fiber diameter does not affect the overall properties of unidirectional tows which are used as input for these unit cells. Even though the separation of scales is observed at $\lambda/d = 50$, it is not clear which homogenization method (i.e. analytical, FEA hexagonal or FEA square) works best for approximation of the explicit models' responses. While the homogenized hexagonal and homogenized analytical model predictions are close to each other in all E and G plots, the results obtained for ν show these results diverging. These homogenized methods work best for predicting the explicit model behavior in some cases: for E_x (CR = 0.05), E_y (CR = 0.05, 0.10), G_{xy} (CR = 0.05, 0.10), E_z (all crimp ratios), G_{vz} (all crimp ratios) and G_{xz} (CR = 0.05, 0.10). On the other hand, the homogenized square model works best for all other elastic constants (except for G_{xy} at CR = 0.15). We recommend performing tow homogenization using the explicit models if possible, or the homogenized analytical model.

Analysis of the effect of crimp ratio on the overall elastic moduli of tows showed that with the increase of crimp ratio, E_x decreases while E_y , G_{xy} , and G_{yz} increase. There are no significant changes in the predictions of E_z or G_{zx} . These results are in agreement with previous publications [11,37,44,45]. Predictions of Poisson's ratios presented no

consistent trends.

In the second part of the paper, we focus on the effective elastic properties of unit cells of woven composites of three architectures: orthogonal, ply-to-ply and plain weave. Two methods are compared: stiffness approximation (Voigt model) and direct FEA. In the former method, the composite unit cell is represented as a collection of sinusoidal tows "connected in parallel". The response of each tow is taken from the first part of the paper based on that tow's crimp ratio (approximated from the geometry analysis). Note that due to the curvilinear shape of the tows their interaction is not taken into account. In the latter method, the composite unit cells are modeled using FEA with homogenized tows. In addition, predictions are compared with experimental measurements of the in-plane Young's moduli in the case of the orthogonal architecture.

The results indicate that the stiffness approximation which does not require expensive FEA simulations of woven unit cells may work as a reasonable first-order approximation for Young's moduli of low-crimp composites (ply-to-ply and plain weave) – the relative error is below 17% when compared with the direct FEA results. However, the predictions produced by this method are not acceptable for high-crimp composites such as the orthogonal configuration – the relative error exceeds 30%. In all cases, the stiffness approximation procedure underestimated the in-plane Young's moduli and overestimated all shear moduli. On the other hand, direct FEA simulation results for the in-plane Young's moduli appear to be in good correspondence with the experimental results – both moduli predictions fall within the range of experimental values.

Even though two-step homogenization of 3D woven composites based on FEA of unit cells relies on accurate reproduction of the reinforcement geometry, which is still a labor-intensive process, the method appears to produce the best predictions when compared with experimental results as is shown in this paper.

Acknowledgements

This material is based upon work supported by the National Science Foundation under Grant No. CMMI-1662098. We are grateful to Adam Ewert for his help with geometric modeling and FEA model preparation for the orthogonal architecture.

Appendix A

Overall stiffness matrix components (GPa) of the wavy tow unit cells (explicit models, normalized wavelength $\lambda/d = 50$):

CR	C11	C12	C13	C21	C22	C23	C31	C32	C33	C44/2	C55/2	C66/2
0.00	100.0	6.007	6.007	6.041	10.00	4.057	6.041	4.057	10.00	0.671	F 00F	F 00F
0.00	198.2	6.037	6.037	6.041	12.29	4.957	6.041	4.957	12.29	3.671	5.095	5.095
0.05	83.89	6.639	5.427	6.638	12.64	5.000	5.427	5.001	12.16	3.782	4.968	5.691
0.10	43.90	6.651	5.451	6.645	13.88	5.163	5.447	5.162	11.97	4.055	4.813	6.953
0.15	29.90	6.844	5.258	6.840	15.59	4.953	5.252	4.951	12.90	4.155	5.077	7.414

References

- Verpoest I, Lomov SV. Virtual textile composites software WiseTex: integration with micro-mechanical, permeability and structural analysis. Compos. Sci. Technol. 2005;65(15–16):2563–74.
- [2] Drach A, Drach B, Tsukrov I. Processing of fiber architecture data for finite element modeling of 3D woven composites. Adv. Eng. Softw. 2014;72:18–27.
- [3] Liu X, Rouf K, Peng B, Yu W. Two-step homogenization of textile composites using mechanics of structure genome. Compos. Struct. 2017;171:252–62.
- [4] Fagiano C, Genet M, Baranger E, Ladevèze P. Computational geometrical and mechanical modeling of woven ceramic composites at the mesoscale. Compos. Struct. 2014;112(1):146–56.
- [5] Tomkova B, Sejnoha M, Novak J, Zeman J. Evaluation of effective thermal conductivities of porous textile Composites. Int. J. Multiscale Comput. Eng. 2008;6(2):153–67.
- [6] de Macedo RQ, Ferreira RTL, Donadon MV, Guedes JM. Elastic properties of unidirectional fiber-reinforced composites using asymptotic homogenization

- techniques. J. Brazilian Soc. Mech. Sci. Eng. 2018;40(5).
- [7] de Macedo RQ, Ferreira RTL, Guedes JM, Donadon MV. Intraply failure criterion for unidirectional fiber reinforced composites by means of asymptotic homogenization. Compos. Struct. 2017;159:335–49.
- [8] Olave M, Vanaerschot A, Lomov SV, Dirk V. Internal geometry variability of two woven composites and related variability of the stiffness. Polym. Compos. 2012;33(8):1335–50.
- [9] Lomov SV, et al. Predictive analyses and experimental validations of effective elastic properties of 2D and 3D woven composites. 13th Eur Conf. Compos. Mater. 2008.
- [10] Vorobiov O, Tabatabaei SA, Lomov SV. Mesh superposition applied to meso-FE modelling of fibre-reinforced composites: cross-comparison of implementations. Int. J. Numer. Methods Eng. 2017;111(11):1003–24.
- [11] Garnich MR, Karami G. Finite element micromechanics for stiffness and strength of wavy fiber composites. J. Compos. Mater. 2004;38(4):273–92.
- [12] Karami G, Garnich M. Effective moduli and failure considerations for composites with periodic fiber waviness. Compos. Struct. 2005;67(4):461–75.
- [13] Karami G, Garnich M. Micromechanical study of thermoelastic behavior of composites with periodic fiber waviness. Compos. Part B Eng. 2005;36(3):241–8.

- [14] Kuksenko D, Böhm HJ, Drach B. Effect of micromechanical parameters of composites with wavy fibers on their effective response under large deformations. Adv. Eng. Softw. 2018;121:206–22.
- [15] Chamis C. Mechanics of composite materials: past, present, and future. J. Compos. Technol. Res. 1989;11(1):3–14.
- [16] Hashin Z, Shtrikman S. A variational approach to the theory of the elastic behaviour of multiphase materials. J. Mech. Phys. Solids 1963;11(42):127–40.
- [17] Hashin Z. Analysis of properties of fiber composites with anisotropic constituents. J. Appl. Mech. 1979;46(3):543–50.
- [18] Tsukrov I, Drach B, Gross TS. Effective stiffness and thermal expansion coefficients of unidirectional composites with fibers surrounded by cylindrically orthotropic matrix layers. Int. J. Eng. Sci. 2012;58:129–43.
- [19] Stig F, Hallström S. Influence of crimp on 3D-woven fibre reinforced composites. Compos. Struct. 2013;95:114–22.
- [20] Naik NK, Ganesh VK. An analytical method for plain weave fabric composites. Composites 1995;26(4):281–9.
- [21] Buchanan S, Grigorash A, Archer E, McIlhagger A, Quinn J, Stewart G. Analytical elastic stiffness model for 3D woven orthogonal interlock composites. Compos. Sci. Technol. 2010;70(11):1597–604.
- [22] Stig F, Hallström S. Spatial modelling of 3D-woven textiles. Compos. Struct. 2012;94(5):1495–502.
- [23] Wucher B, et al. Non-conformal finite element homogenization applied to woven composites with complex textile architectures. 20th Int Conf. Compos. Mater. 2015. p. 19–24.
- [24] Bayraktar H, et al. Forming and performance analysis of a 3D-woven composite curved beam using meso-scale FEA. Rochester, NH: Sampe Journal; 2015. p. 23–9.
- [25] Green SD, Matveev MY, Long AC, Ivanov D, Hallett SR. Mechanical modelling of 3D woven composites considering realistic unit cell geometry. Compos. Struct. 2014;118(1):284–93.
- [26] Lomov SV, Perie G, Ivanov D, Verpoest I, Marsal D. Modeling three-dimensional fabrics and three-dimensional reinforced composites: challenges and solutions. Text. Res. J. 2011;81(1):28–41.
- [27] Silva H, Drach B. Applicability of two-step homogenization in high-crimp woven composites. Proc. Am. Soc. Compos. – 33rd Tech Conf. ASC 2018. 2018.
- [28] Cooke W. Mathematics of Crimping PhD Thesis University of Oxford; 2000.
- [29] Zhong S, Guo L, Liu G, Zhang L, Pan S. A random waveness model for the stiffness and strength evaluation of 3D woven composites. Compos. Struct. 2016;152:1024–32.

- [30] Ballard MK, Whitcomb JD. Stress analysis of 3D textile composites using high performance computing: new insights and challenges. IOP Conf. Ser. Mater. Sci. Eng. 2018;406. 012004.
- [31] Llorca J, Segurado J. A numerical approximation to the elastic properties of sphere reinforced composites. J. Mech. Phys. Solids 2002;50:2107–21.
- [32] Drach B, Tsukrov I, Trofimov A. Comparison of full field and single pore approaches to homogenization of linearly elastic materials with pores of regular and irregular shapes. Int. J. Solids Struct. 2016;96:48–63.
- [33] Xia Z, Zhang Y, Ellyin F. A unified periodical boundary conditions for representative volume elements of composites and applications. Int. J. Solids Struct. 2003;40(8):1907–21.
- [34] Taubin G. A signal processing approach to fair surface design. Proc. 22nd Annu Conf. Comput. Graph. Interact. Tech. - SIGGRAPH. 1995. p. 351–8.
- [35] Drach B, Tsukrov I, Trofimov A, Gross T, Drach A. Comparison of stress-based failure criteria for prediction of curing induced damage in 3D woven composites. Compos. Struct. 2018;189:366–77.
- [36] Kuksenko D, Drach B. Effective conductivity of materials with continuous curved fibers. Int. J. Eng. Sci. 2017;118:70–81.
- [37] Drach B, Kuksenko D, Sevostianov I. Effect of a curved fiber on the overall material stiffness. Int. J. Solids Struct. 2016;100–101:211–22.
- [38] Wang Y, Sun X. Digital-element simulation of textile processes. Compos. Sci. Technol. 2001;61(2):311–9.
- [39] Zhou G, Sun X, Wang Y. Multi-chain digital element analysis in textile mechanics. Compos. Sci. Technol. 2004;64(2):239–44.
- [40] Miao Y, Zhou E, Wang Y, Cheeseman BA. Mechanics of textile composites: microgeometry. Compos. Sci. Technol. 2008;68(7–8):1671–8.
- [41] Rueden CT, et al. ImageJ2: imageJ for the next generation of scientific image data. BMC Bioinf 2017;18(1):1–26.
- [42] Drach B, Drach A, Tsukrov I, Penverne M, Lapusta Y. Finite element models of 3D woven composites based on numerically generated micro-geometry of reinforcement. Proc. Am. Soc. Compos. 29th Tech. Conf. 2014.
- [43] Vyshenska K. Numerical and experimental studies of mechanical behavior and cure induced stresses in 3D carbon/epoxy composites Master's Thesis University of New Hampshire: 2014.
- [44] Zhu J, Wang J, Zu L. Influence of out-of-plane ply waviness on elastic properties of composite laminates under uniaxial loading. Compos. Struct. 2015;132:440–50.
- [45] Whitcomb JD, Tang X. Effective moduli of woven composites. J. Compos. Mater. 2001;35(23):2127–44.